

Measurement of J/ψ Azimuthal Anisotropy in Au + Au Collisions at $\sqrt{s_{NN}} = 200$ GeV

L. Adamczyk,¹ J.K. Adkins,²³ G. Agakishiev,²¹ M.M. Aggarwal,³⁴ Z. Ahammed,⁵³ I. Alekseev,¹⁹ J. Alford,²² C.D. Anson,³¹ A. Aparin,²¹ D. Arkhipkin,⁴ E. Aschenauer,⁴ G.S. Averichev,²¹ J. Balewski,²⁶ A. Banerjee,⁵³ Z. Barnovska,¹⁴ D.R. Beavis,⁴ R. Bellwied,⁴⁹ M.J. Betancourt,²⁶ R.R. Betts,¹⁰ A. Bhasin,²⁰ A.K. Bhati,³⁴ P. Bhattarai,⁴⁸ H. Bichsel,⁵⁵ J. Bielcik,¹³ J. Bielcikova,¹⁴ L.C. Bland,⁴ I.G. Bordyuzhin,¹⁹ W. Borowski,⁴⁵ J. Bouchet,²² A.V. Brandin,²⁹ S.G. Brovko,⁶ E. Bruna,⁵⁷ S. Bültmann,³² I. Bunzarov,²¹ T.P. Burton,⁴ J. Butterworth,⁴⁰ X.Z. Cai,⁴⁴ H. Caines,⁵⁷ M. Calderón de la Barca Sánchez,⁶ D. Cebra,⁶ R. Cendejas,³⁵ M.C. Cervantes,⁴⁷ P. Chaloupka,¹³ Z. Chang,⁴⁷ S. Chattopadhyay,⁵³ H.F. Chen,⁴² J.H. Chen,⁴⁴ J.Y. Chen,⁹ L. Chen,⁹ J. Cheng,⁵⁰ M. Cherney,¹² A. Chikanian,⁵⁷ W. Christie,⁴ P. Chung,¹⁴ J. Chwastowski,¹¹ M.J.M. Coddington,⁴⁸ R. Corliss,²⁶ J.G. Cramer,⁵⁵ H.J. Crawford,⁵ X. Cui,⁴² S. Das,¹⁶ A. Davila Leyva,⁴⁸ L.C. De Silva,⁴⁹ R.R. Debbé,⁴ T.G. Dedovich,²¹ J. Deng,⁴³ R. Derradi de Souza,⁸ S. Dhamija,¹⁸ B. di Ruzza,⁴ L. Didenko,⁴ F. Ding,⁶ A. Dion,⁴ P. Djawotho,⁴⁷ X. Dong,²⁵ J.L. Drachenberg,⁵² J.E. Draper,⁶ C.M. Du,²⁴ L.E. Dunkelberger,⁷ J.C. Dunlop,⁴ L.G. Efimov,²¹ M. Elnimr,⁵⁶ J. Engelage,⁵ G. Eppley,⁴⁰ L. Eun,²⁵ O. Evdokimov,¹⁰ R. Fatemi,²³ S. Fazio,⁴ J. Fedorisin,²¹ R.G. Fersch,²³ P. Filip,²¹ E. Finch,⁵⁷ Y. Fisyak,⁴ E. Flores,⁶ C.A. Gagliardi,⁴⁷ D.R. Gangadharan,³¹ D. Garand,³⁷ F. Geurts,⁴⁰ A. Gibson,⁵² S. Gliske,² O.G. Grebenyuk,²⁵ D. Grosnick,⁵² A. Gupta,²⁰ S. Gupta,²⁰ W. Guryn,⁴ B. Haag,⁶ O. Hajkova,¹³ A. Hamed,⁴⁷ L.-X. Han,⁴⁴ J.W. Harris,⁵⁷ J.P. Hays-Wehle,²⁶ S. Heppelmann,³⁵ A. Hirsch,³⁷ G.W. Hoffmann,⁴⁸ D.J. Hofman,¹⁰ S. Horvat,⁵⁷ B. Huang,⁴ H.Z. Huang,⁷ P. Huck,⁹ T.J. Humanic,³¹ G. Igo,⁷ W.W. Jacobs,¹⁸ C. Jena,³⁰ E.G. Judd,⁵ S. Kabana,⁴⁵ K. Kang,⁵⁰ J. Kapitan,¹⁴ K. Kauder,¹⁰ H.W. Ke,⁹ D. Keane,²² A. Kechechyan,²¹ A. Kesich,⁶ D.P. Kikola,³⁷ J. Kiryluk,²⁵ I. Kisel,²⁵ A. Kisiel,⁵⁴ S.R. Klein,²⁵ D.D. Koetke,⁵² T. Kollegger,¹⁵ J. Konzer,³⁷ I. Koralt,³² W. Korsch,²³ L. Kotchenda,²⁹ P. Kravtsov,²⁹ K. Krueger,² I. Kulakov,²⁵ L. Kumar,²² M.A.C. Lamont,⁴ J.M. Landgraf,⁴ K.D. Landry,⁷ S. LaPointe,⁵⁶ J. Lauret,⁴ A. Lebedev,⁴ R. Lednicky,²¹ J.H. Lee,⁴ W. Leight,²⁶ M.J. LeVine,⁴ C. Li,⁴² W. Li,⁴⁴ X. Li,³⁷ X. Li,⁴⁶ Y. Li,⁵⁰ Z.M. Li,⁹ L.M. Lima,⁴¹ M.A. Lisa,³¹ F. Liu,⁹ T. Ljubicic,⁴ W.J. Llope,⁴⁰ R.S. Longacre,⁴ Y. Lu,⁴² X. Luo,⁹ A. Luszczak,¹¹ G.L. Ma,⁴⁴ Y.G. Ma,⁴⁴ D.M.M.D. Madagodagettige Don,¹² D.P. Mahapatra,¹⁶ R. Majka,⁵⁷ S. Margetis,²² C. Markert,⁴⁸ H. Masui,²⁵ H.S. Matis,²⁵ D. McDonald,⁴⁰ T.S. McShane,¹² S. Mioduszewski,⁴⁷ M.K. Mitrovski,⁴ Y. Mohammed,⁴⁷ B. Mohanty,³⁰ M.M. Mondal,⁴⁷ M.G. Munhoz,⁴¹ M.K. Mustafa,³⁷ M. Naglis,²⁵ B.K. Nandi,¹⁷ Md. Nasim,⁵³ T.K. Nayak,⁵³ J.M. Nelson,³ L.V. Nogach,³⁶ J. Novak,²⁸ G. Odyniec,²⁵ A. Ogawa,⁴ K. Oh,³⁸ A. Ohlson,⁵⁷ V. Okorokov,²⁹ E.W. Oldag,⁴⁸ R.A.N. Oliveira,⁴¹ D. Olson,²⁵ M. Pachr,¹³ B.S. Page,¹⁸ S.K. Pal,⁵³ Y.X. Pan,⁷ Y. Pandit,¹⁰ Y. Panebratsev,²¹ T. Pawlak,⁵⁴ B. Pawlik,³³ H. Pei,¹⁰ C. Perkins,⁵ W. Peryt,⁵⁴ P. Pile,⁴ M. Planinic,⁵⁸ J. Pluta,⁵⁴ N. Poljak,⁵⁸ J. Porter,²⁵ A.M. Poskanzer,²⁵ C.B. Powell,²⁵ C. Pruneau,⁵⁶ N.K. Pruthi,³⁴ M. Przybycien,¹ P.R. Pujahari,¹⁷ J. Putschke,⁵⁶ H. Qiu,²⁵ S. Ramachandran,²³ R. Raniwala,³⁹ S. Raniwala,³⁹ R.L. Ray,⁴⁸ C.K. Riley,⁵⁷ H.G. Ritter,²⁵ J.B. Roberts,⁴⁰ O.V. Rogachevskiy,²¹ J.L. Romero,⁶ J.F. Ross,¹² L. Ruan,⁴ J. Rusnak,¹⁴ N.R. Sahoo,⁵³ P.K. Sahu,¹⁶ I. Sakrejda,²⁵ S. Salur,²⁵ A. Sandacz,⁵⁴ J. Sandweiss,⁵⁷ E. Sangaline,⁶ A. Sarkar,¹⁷ J. Schambach,⁴⁸ R.P. Scharenberg,³⁷ A.M. Schmah,²⁵ B. Schmidke,⁴ N. Schmitz,²⁷ T.R. Schuster,¹⁵ J. Seger,¹² P. Seyboth,²⁷ N. Shah,⁷ E. Shaliev,²¹ M. Shao,⁴² B. Sharma,³⁴ M. Sharma,⁵⁶ S.S. Shi,⁹ Q.Y. Shou,⁴⁴ E.P. Sichtermann,²⁵ R.N. Singaraju,⁵³ M.J. Skoby,¹⁸ D. Smirnov,⁴ N. Smirnov,⁵⁷ D. Solanki,³⁹ P. Sorensen,⁴ U.G. deSouza,⁴¹ H.M. Spinka,² B. Srivastava,³⁷ T.D.S. Stanislaus,⁵² J.R. Stevens,²⁶ R. Stock,¹⁵ M. Strikhanov,²⁹ B. Stringfellow,³⁷ A.A.P. Suaide,⁴¹ M.C. Suarez,¹⁰ M. Sumbera,¹⁴ X.M. Sun,²⁵ Y. Sun,⁴² Z. Sun,²⁴ B. Surrøw,⁴⁶ D.N. Svirida,¹⁹ T.J.M. Symons,²⁵ A. Szanto de Toledo,⁴¹ J. Takahashi,⁸ A.H. Tang,⁴ Z. Tang,⁴² L.H. Tarini,⁵⁶ T. Tarnowsky,²⁸ J.H. Thomas,²⁵ J. Tian,⁴⁴ A.R. Timmins,⁴⁹ D. Tlusty,¹⁴ M. Tokarev,²¹ S. Trentalange,⁷ R.E. Tribble,⁴⁷ P. Tribedy,⁵³ B.A. Trzeciak,⁵⁴ O.D. Tsai,⁷ J. Turnau,³³ T. Ullrich,⁴ D.G. Underwood,² G. Van Buren,⁴ G. van Nieuwenhuizen,²⁶ J.A. Vanfossen, Jr.,²² R. Varma,¹⁷ G.M.S. Vasconcelos,⁸ F. Videbæk,⁴ Y.P. Viyogi,⁵³ S. Vokal,²¹ S.A. Voloshin,⁵⁶ A. Vossen,¹⁸ M. Wada,⁴⁸ F. Wang,³⁷ G. Wang,⁷ H. Wang,⁴ J.S. Wang,²⁴ Q. Wang,³⁷ X.L. Wang,⁴² Y. Wang,⁵⁰ G. Webb,²³ J.C. Webb,⁴ G.D. Westfall,²⁸ C. Whitten, Jr.,⁷ H. Wieman,²⁵ S.W. Wissink,¹⁸ R. Witt,⁵¹ Y.F. Wu,⁹ Z. Xiao,⁵⁰ W. Xie,³⁷ K. Xin,⁴⁰ H. Xu,²⁴ N. Xu,²⁵ Q.H. Xu,⁴³ W. Xu,⁷ Y. Xu,⁴² Z. Xu,⁴ L. Xue,⁴⁴ Y. Yang,²⁴ Y. Yang,⁹ P. Yepes,⁴⁰ L. Yi,³⁷ K. Yip,⁴ I.-K. Yoo,³⁸ M. Zawisza,⁵⁴ H. Zbroszczyk,⁵⁴ J.B. Zhang,⁹ S. Zhang,⁴⁴ X.P. Zhang,⁵⁰ Y. Zhang,⁴² Z.P. Zhang,⁴² F. Zhao,⁷ J. Zhao,⁴⁴ C. Zhong,⁴⁴ X. Zhu,⁵⁰ Y.H. Zhu,⁴⁴ Y. Zoukarnieva,²¹ and M. Zyzak²⁵

(STAR Collaboration)

- ¹AGH University of Science and Technology, Cracow, Poland
²Argonne National Laboratory, Argonne, Illinois 60439, USA
³University of Birmingham, Birmingham, United Kingdom
⁴Brookhaven National Laboratory, Upton, New York 11973, USA
⁵University of California, Berkeley, California 94720, USA
⁶University of California, Davis, California 95616, USA
⁷University of California, Los Angeles, California 90095, USA
⁸Universidade Estadual de Campinas, Sao Paulo, Brazil
⁹Central China Normal University (HZNU), Wuhan 430079, China
¹⁰University of Illinois at Chicago, Chicago, Illinois 60607, USA
¹¹Cracow University of Technology, Cracow, Poland
¹²Creighton University, Omaha, Nebraska 68178, USA
¹³Czech Technical University in Prague, FNSPE, Prague 115 19, Czech Republic
¹⁴Nuclear Physics Institute AS CR, 250 68 Řež/Prague, Czech Republic
¹⁵University of Frankfurt, Frankfurt, Germany
¹⁶Institute of Physics, Bhubaneswar 751005, India
¹⁷Indian Institute of Technology, Mumbai, India
¹⁸Indiana University, Bloomington, Indiana 47408, USA
¹⁹Alikhanov Institute for Theoretical and Experimental Physics, Moscow, Russia
²⁰University of Jammu, Jammu 180001, India
²¹Joint Institute for Nuclear Research, Dubna 141 980, Russia
²²Kent State University, Kent, Ohio 44242, USA
²³University of Kentucky, Lexington, Kentucky 40506-0055, USA
²⁴Institute of Modern Physics, Lanzhou, China
²⁵Lawrence Berkeley National Laboratory, Berkeley, California 94720, USA
²⁶Massachusetts Institute of Technology, Cambridge, Massachusetts 02139-4307, USA
²⁷Max-Planck-Institut für Physik, Munich, Germany
²⁸Michigan State University, East Lansing, Michigan 48824, USA
²⁹Moscow Engineering Physics Institute, Moscow, Russia
³⁰National Institute of Science and Education and Research, Bhubaneswar 751005, India
³¹Ohio State University, Columbus, Ohio 43210, USA
³²Old Dominion University, Norfolk, Virginia 23529, USA
³³Institute of Nuclear Physics PAN, Cracow, Poland
³⁴Panjab University, Chandigarh 160014, India
³⁵Pennsylvania State University, University Park, Pennsylvania 16802, USA
³⁶Institute of High Energy Physics, Protvino, Russia
³⁷Purdue University, West Lafayette, Indiana 47907, USA
³⁸Pusan National University, Pusan, Republic of Korea
³⁹University of Rajasthan, Jaipur 302004, India
⁴⁰Rice University, Houston, Texas 77251, USA
⁴¹Universidade de Sao Paulo, Sao Paulo, Brazil
⁴²University of Science and Technology of China, Hefei 230026, China
⁴³Shandong University, Jinan, Shandong 250100, China
⁴⁴Shanghai Institute of Applied Physics, Shanghai 201800, China
⁴⁵SUBATECH, Nantes, France
⁴⁶Temple University, Philadelphia, Pennsylvania 19122, USA
⁴⁷Texas A&M University, College Station, Texas 77843, USA
⁴⁸University of Texas, Austin, Texas 78712, USA
⁴⁹University of Houston, Houston, Texas 77204, USA
⁵⁰Tsinghua University, Beijing 100084, China
⁵¹United States Naval Academy, Annapolis, Maryland 21402, USA
⁵²Valparaiso University, Valparaiso, Indiana 46383, USA
⁵³Variable Energy Cyclotron Centre, Kolkata 700064, India
⁵⁴Warsaw University of Technology, Warsaw, Poland
⁵⁵University of Washington, Seattle, Washington 98195, USA
⁵⁶Wayne State University, Detroit, Michigan 48201, USA
⁵⁷Yale University, New Haven, Connecticut 06520, USA

⁵⁸*University of Zagreb, Zagreb, HR-10002, Croatia*

(Received 13 December 2012; revised manuscript received 10 May 2013; published 2 August 2013)

The measurement of J/ψ azimuthal anisotropy is presented as a function of transverse momentum for different centralities in Au + Au collisions at $\sqrt{s_{NN}} = 200$ GeV. The measured J/ψ elliptic flow is consistent with zero within errors for transverse momentum between 2 and 10 GeV/ c . Our measurement suggests that J/ψ particles with relatively large transverse momenta are not dominantly produced by coalescence from thermalized charm quarks, when comparing to model calculations.

DOI: [10.1103/PhysRevLett.111.052301](https://doi.org/10.1103/PhysRevLett.111.052301)

PACS numbers: 25.75.Cj, 12.38.Mh, 14.40.Pq

Quantum chromodynamics (QCD) predicts a quark-gluon plasma (QGP) phase at extremely high temperature and/or density, consisting of deconfined quarks and gluons. Over the past twenty years, heavy quarkonia production in hot and dense nuclear matter has been a topic attracting growing interest. In relativistic heavy-ion collisions the $c\bar{c}$ bound state is subject to dissociation due to the color screening effect in the deconfined medium. As a consequence, the production of the J/ψ is expected to be suppressed compared to proton + proton ($p + p$) collisions scaled by number of binary collisions, and such suppression has been proposed as a signature of QGP formation [1]. However, the J/ψ suppression observed in experiments [2–6] can also be affected by additional cold [7,8] and hot [9–14] nuclear effects. In particular, the recombination of the J/ψ from a thermalized charm quark and its antiquark [11–14] has not been unambiguously established experimentally at the top RHIC energy. By measuring J/ψ azimuthal anisotropy, especially its second Fourier coefficient v_2 (elliptic flow), one may infer the relative contribution of J/ψ particles from direct perturbative QCD (pQCD) processes and from recombination. J/ψ particles produced from direct pQCD processes, which do not have initial collective motion, should have little azimuthal preference. In noncentral collisions, the produced J/ψ particles will then gain limited azimuthal anisotropy from azimuthally different absorption due to the different path lengths in azimuth. On the other hand, J/ψ particles produced from recombination of thermalized charm quarks will inherit the flow of charm quarks, exhibiting considerable flow.

Many models that describe the experimental results of heavy-ion collisions depend on the assumption that light flavor quarks in the medium reach thermalization on a short time scale (~ 0.5 fm/ c) [15,16]. However, this rapid full thermalization has not been directly certified. The flow pattern of heavy quarks provides a unique tool to test the thermalization. With much larger mass than that of light quarks, heavy quarks are more resistant to having their velocity changed, and are thus expected to thermalize much more slowly than light partons. If charm quarks are observed to have sizable collective motion, then light partons, which dominate the medium, should be fully thermalized. The charm quark flow can be measured through open [17] and closed charm particles. The J/ψ is the most prominent for experiment among the latter.

However, because the J/ψ production mechanism is not well understood, there is significant uncertainty associated with this probe, since only J/ψ particles from recombination of charm quarks inherit their flow. A detailed comparison between experimental measurements and models on J/ψ v_2 vs transverse momentum (p_T) and centrality, in addition to nuclear modification factor, will shed light on the J/ψ production mechanism and charm quark flow.

This analysis benefits from a large amount of data taken during the RHIC [18] $\sqrt{s_{NN}} = 200$ GeV Au + Au run in the year 2010 by the new data acquisition system of STAR [19], capable of an event rate up to 1 kHz. In addition, the newly installed time of flight (TOF) detector [20] allows STAR to improve electron identification, and background electrons from photon conversion are reduced by one order of magnitude due to less material around the center of the detector setup. The data presented consist of 360 million minimum bias (MB) events triggered by the coincidence of two vertex position detectors [21], 270 million central events triggered by a large hit multiplicity in the TOF detector [20], and a set of high tower events triggered by signals in the towers of the barrel electromagnetic calorimeter (BEMC) [22] exceeding certain thresholds (2.6, 3.5, 4.2, and 5.9 GeV). The high tower sample is equivalent to approximately 7 billion MB events for J/ψ production in the high- p_T region. In addition, in order to cope with the large data volume coming from collisions at high luminosity, a high level trigger (HLT) was implemented to reconstruct charged tracks online, select events with J/ψ candidates and tag them for fast analysis. There are 16 million J/ψ enriched events selected by the HLT.

The J/ψ particles were reconstructed through the $J/\psi \rightarrow e^+e^-$ channel, which has a branching ratio of 5.9%. The daughter tracks of the J/ψ particles were required to have more than 20 hits in the time projection chamber (TPC) [23], and a distance of closest approach less than 1 cm from the primary vertex. Low-momentum electrons and positrons can be separated from hadrons by selecting on the inverse velocity ($0.97 < 1/\beta < 1.03$), which is calculated from the time of flight measured by the TOF detector [20] and the path length measured by the TPC. At large momentum ($p > 1.5$ GeV/ c), with the energy measured by towers from the BEMC [22], a cut of the momentum to energy ratio ($0.3 < p/E < 1.5$) was applied to select electrons and positrons. The electrons and

TABLE I. Event plane resolution (R) for different centralities.

Centrality (%)	0–10	10–20	20–30	30–40	40–50	50–60	60–70	70–80
R	0.600	0.748	0.805	0.787	0.719	0.608	0.478	0.364

positrons were then identified by their specific energy loss ($\langle dE/dx \rangle$) inside the TPC. More than 15 TPC hits were required to calculate $\langle dE/dx \rangle$. The $\langle dE/dx \rangle$ cut is asymmetric around the expected value for electrons, because the lower side is where the hadron $\langle dE/dx \rangle$ lies. It also varies according to whether the candidate track passes the $1/\beta$ and/or p/E cut to optimize efficiency and purity. The combination of cuts on $1/\beta$, p/E , and $\langle dE/dx \rangle$ enables electron and positron identification in a wide momentum range. Our measured J/ψ particles cover the rapidity range $-1 < y < 1$, favoring J/ψ particles near $y = 0$ because of detection efficiency variation due to acceptance and decay kinematics. A total of just over 13 000 J/ψ particles were reconstructed in the entire p_T range of 0–10 GeV/ c .

The following method has been used to calculate the v_2 of the J/ψ . First, measurements of $\phi-\Psi$, ranging from 0 to π , were divided into 10 bins. Here ϕ is the azimuthal angle of the J/ψ candidate, and Ψ is the azimuthal angle of the event plane reconstructed from TPC tracks with the azimuthally nonuniform detector efficiency corrected for [24]. The event plane resolution [24] (R) is different for different centrality ranges, as listed in Table I. Then two bins at supplementary angles were combined into one. For example, the bin at 0–0.1 π is combined with 0.9 π – π , and the invariant mass distribution of electron and positron pairs in this combined $\phi-\Psi$ bin is shown in the top of Fig. 1. To avoid bias from different event plane resolution for different centrality, entries in the histogram were weighted by $1/R$ accordingly [25]. The weighted J/ψ yield within this combined $\phi-\Psi$ bin was obtained by fitting the e^+e^- invariant mass distribution with a Crystal Ball function [26] signal on top of a second order polynomial background, as shown in the plot. The Crystal Ball function connects a Gaussian core with a power-law tail at low mass to account for daughter energy loss fluctuations and J/ψ radiative decays. Then v_2 was obtained by fitting the weighted J/ψ yield vs $\phi-\Psi$ with a functional form of $A[1 + 2v_2 \cos\{2(\phi-\Psi)\}]$, as shown in the bottom of Fig. 1. Finally, the observed v_2 was scaled by $\langle 1/R \rangle$ to obtain the true v_2 [25].

Three dominant sources of systematic error have been investigated for this measurement: assumptions in the v_2 calculation method, hadron contamination for the daughter e^+e^- pairs, and the nonflow effect. The first source can be estimated from the difference in v_2 calculated by methods with different assumptions. Two other methods are used here. One is similar to the original method, except that the J/ψ yield in each combined $\phi-\Psi$ bin was not obtained from fitting, but from subtracting the like-sign background from unlike-sign distribution within the

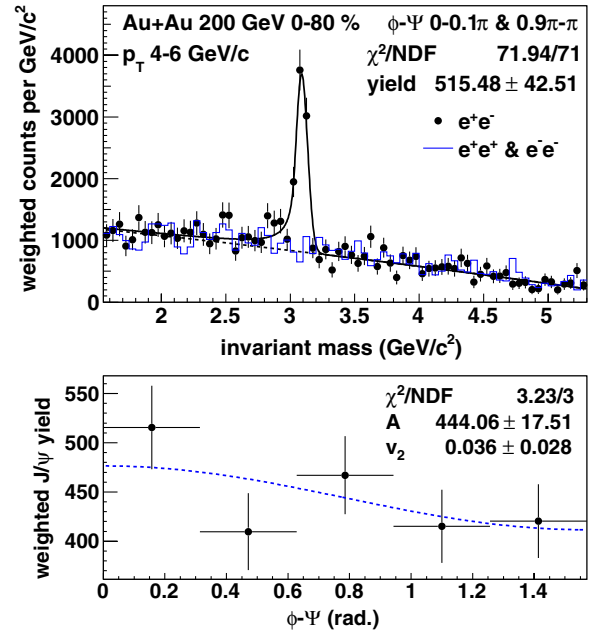


FIG. 1 (color online). Top: $1/R$ weighted invariant mass spectrum of electron and positron pairs for $\phi-\Psi$ in 0–0.1 π and 0.9 π – π , $4 < p_T < 6$ GeV/ c , in 0%–80% central collisions. The points are unlike-sign pairs with the J/ψ signal, fitted by a Crystal Ball plus second order polynomial function. The polynomial background component of the fit is shown by the dashed line. The solid line histogram shows the like-sign background. Bottom: $1/R$ weighted J/ψ yield vs $\phi-\Psi$ with fitted v_2 .

possible invariant mass range of the J/ψ (2.9–3.3 GeV/ c^2). In the other method, the overall v_2 of both signal and background was measured first as a function of invariant mass, and then it was fitted with an average of J/ψ v_2 and background v_2 weighted by their respective yields vs invariant mass [27]. The systematic error from hadron contamination can be estimated from the difference in calculated v_2 with different electron (positron) identification cuts. While the original cuts aim for the best J/ψ significance, a purer electron (positron) sample can be obtained from a set of tighter cuts. The overall systematic uncertainty for the first two sources was estimated from the maximum difference between the calculated v_2 with the $3 \times 2 = 6$ combinations of v_2 methods and electron (positron) identification cut sets mentioned above. Besides elliptic flow, there are also some other two- and many-particle correlations due to, for example, resonance decay and jet production. When v_2 of a particle is measured, other particles having nonflow correlations with the measured particle are more likely to be azimuthally nearby, drawing the reconstructed event plane closer to the measured particle, and make the measured v_2 larger than its real value. To estimate this nonflow influence on the v_2 measurement, a method of scaling nonflow in $p + p$ collisions to that in Au + Au collisions [28] was employed. This method assumes that 1) J/ψ -hadron correlation in

$p + p$ collisions is entirely due to nonflow, and 2) the nonflow correlation to other particles per J/ψ in Au + Au collisions is similar to that in $p + p$ collisions. Under these assumptions, it can be deduced that the nonflow influence on measured J/ψ v_2 in Au + Au collisions is $\langle \sum_i \cos 2(\phi_{J/\psi} - \phi_i) \rangle / M \bar{v}_2$. Here, the sum is over all measured charged hadrons and the average is over J/ψ particles in $p + p$ collisions. M and \bar{v}_2 are the multiplicity and average elliptic flow of charged hadrons in Au + Au collisions, respectively. Since the away side correlation may be greatly modified by the medium in heavy-ion collisions, this procedure gives an upper limit of the nonflow effect. Detector acceptance and efficiency variation with p_T , centrality, and rapidity may lead to a biased J/ψ sample, which may induce some systematic effects when v_2 also changes with these parameters. But these effects are estimated to be negligible compared to statistical errors.

Figure 2 shows J/ψ v_2 as a function of transverse momentum for different centralities. Due to the nonflow effect, the real v_2 can be lower than the measured value shown in the plot. The boxes indicate the maximum magnitude of the nonflow influence. Data from the central trigger, minimum bias trigger and high tower triggers are used for the 0%–10% most central bin, while only minimum bias and high tower triggered events are used for other centrality bins. Considering errors and the magnitude of nonflow, J/ψ v_2 is consistent with 0 for $p_T > 2$ GeV/c for all measured centrality bins. Light particles usually have a larger v_2 in the intermediate centrality than in the most central and peripheral collisions. This can be explained by a larger initial spatial eccentricity in the intermediate centrality, which is transferred into final state momentum anisotropy due to different pressure gradients in different directions, when

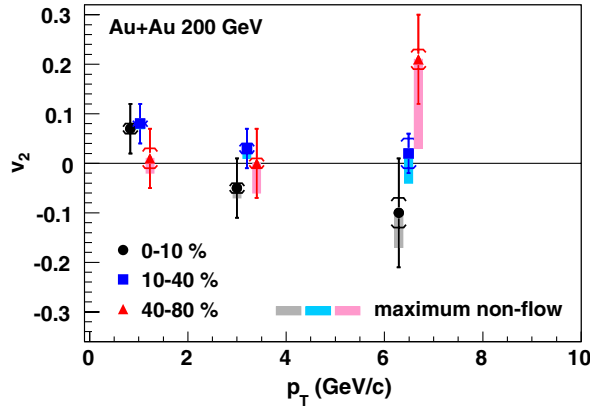


FIG. 2 (color online). v_2 vs p_T for J/ψ particles in different centrality bins. The brackets represent systematic errors estimated from differences between different methods and cuts. The boxes show the estimated maximum possible range of v_2 if the nonflow influence is corrected (see text). The p_T bins for J/ψ particles are 0–2, 2–5, and 5–10 GeV/c. The mean p_T in each bin for the J/ψ sample used for v_2 calculation is drawn, but is shifted a little for some centralities so that all points can be seen clearly.

there are sufficient interactions in the medium. However, no strong centrality dependence for J/ψ v_2 has been observed with the statistical significance of the data.

The top panel of Fig. 3 shows J/ψ v_2 for 0%–80% central collisions as a function of transverse momentum. For reference, two other sets of v_2 measurements are also plotted, one is for charged hadrons (dominated by pions) [29] and the other is for the ϕ meson [30] which is heavier than the pion but not as heavy as the J/ψ . Unlike v_2 of hadrons consisting of light quarks, J/ψ v_2 at $p_T > 2$ GeV/c is found to be consistent with zero within statistical errors. However, the significant mass difference between the J/ψ and light particles makes the direct comparison of v_2 vs p_T less conclusive. For example, for the same velocity at $y = 0$, the p_T of J/ψ particles at 3.0 GeV/c corresponds to p_T of pions (ϕ) at 0.14 (1.0) GeV/c. Thus, comparisons between the experimental result and theoretical calculations are needed.

In the bottom panel of Fig. 3, a comparison is made between the measured J/ψ v_2 and various theoretical calculations, and a quantitative level of difference is shown in Table II by χ^2/NDF and the p value. v_2 of J/ψ particles produced by initial pQCD processes is predicted to stay

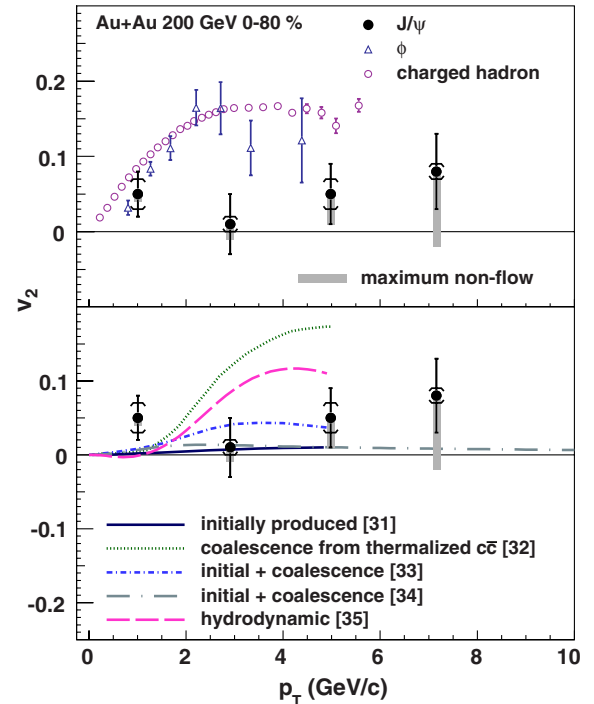


FIG. 3 (color online). v_2 vs p_T for J/ψ particles in 0%–80% central events comparing with charged hadrons [29] and the ϕ meson [30] (upper panel) and theoretical calculations [31–35] (lower panel). The brackets represent systematic errors estimated from differences between different methods and cuts. The boxes show the estimated maximum possible range of v_2 if the nonflow influence is corrected. The p_T bins for J/ψ particles are 0–2, 2–4, 4–6, and 6–10 GeV/c, and the mean p_T in each bin for the J/ψ sample used for v_2 calculation is drawn.

TABLE II. Difference between model calculations and data (where NDF stands for the number of degrees of freedom). The p value is the probability of observing a χ^2 that exceeds the current measured χ^2 by chance, even for a correct model. The estimated upper limit of nonflow effect is not included in this calculation.

Theoretical calculation	χ^2/NDF	p value
Initially produced [31]	2.6/3	4.6×10^{-1}
Coalescence from thermalized $c\bar{c}$ [32]	16.2/3	1.0×10^{-3}
Initial + coalescence [33]	2.0/3	5.8×10^{-1}
Initial + coalescence [34]	4.2/4	3.8×10^{-1}
Hydrodynamic [35]	7.0/3	7.2×10^{-2}

close to zero [31]. Although anomalous suppression in the hot medium due to color screening are considered in the model, the azimuthally different suppression along the different path lengths in azimuth leads to a limited v_2 beyond the sensitivity of the current measurement. On the contrary, if charm quarks get fully thermalized and J/ψ particles are produced by coalescence from the thermalized flowing charm quarks at the freeze-out, the v_2 of the J/ψ is predicted to reach almost the same maximum magnitude as v_2 of light flavor mesons, although at a larger p_T (around 4 GeV/ c) due to the significantly larger mass of the J/ψ [32]. This is nearly 3σ above the measurement for $p_T > 2$ GeV/ c , leading to a large χ^2/NDF of 16.2/3 and a small p value of 1.0×10^{-3} , and is, thus, inconsistent with the data. Models that include J/ψ particles from both initial production and coalescence production in the transport model [31,36] predict a much smaller v_2 [33,34], and are consistent with our measurement. In these models, J/ψ particles are formed continuously through the system evolution rather than at the freeze-out, so many J/ψ particles could be formed from charm quarks whose v_2 has still not fully developed. Furthermore, the initial production of J/ψ particles with very limited v_2 dominates at high p_T , thus, the overall J/ψ v_2 does not rise rapidly as for light hadrons. This kind of model also describes the measured J/ψ nuclear modification factor over a wide range of p_T and centrality [5]. The hydrodynamic model, which assumes local thermal equilibrium, can be tuned to describe v_2 for light hadrons, but it predicts a J/ψ v_2 that rises strongly with p_T in the region $p_T < 4$ GeV/ c , and thus, fails to describe the main feature of the data [35]. For heavy particles such as the J/ψ , hydrodynamic predictions suffer from large uncertainties related to viscous corrections (δf) at freeze-out and the assumed freeze-out time or temperature.

In summary, J/ψ elliptic flow is presented as a function of transverse momentum for different centralities in $\sqrt{s_{NN}} = 200$ GeV Au + Au collisions. Unlike light flavor hadrons, J/ψ v_2 at $p_T > 2$ GeV/ c is consistent with zero within statistical errors. Comparing to model calculations, the measured J/ψ v_2 values disfavor the scenario that J/ψ particles with $p_T > 2$ GeV/ c are produced dominantly by

coalescence from (anti-)charm quarks which are thermalized and flow with the medium.

We thank the RHIC Operations Group and RCF at BNL, the NERSC Center at LBNL and the Open Science Grid consortium for providing resources and support. This work was supported in part by the Offices of NP and HEP within the U.S. DOE Office of Science, the U.S. NSF, the Sloan Foundation; CNRS/IN2P3, FAPESP CNPq of Brazil; Ministry of Education and Science of the Russian Federation; NNSFC, CAS, MoST, and MoE of China; GA and MSMT of the Czech Republic; FOM and NWO of the Netherlands; DAE, DST, and CSIR of India; Polish Ministry of Science and Higher Education; National Research Foundation (NRF-2012004024), Ministry of Science, Education, and Sports of the Republic of Croatia; and RosAtom of Russia.

-
- [1] T. Matsui and H. Satz, *Phys. Lett. B* **178**, 416 (1986).
 - [2] M. C. Abreu *et al.*, *Phys. Lett. B* **499**, 85 (2001).
 - [3] A. Adare *et al.*, *Phys. Rev. Lett.* **98**, 232301 (2007).
 - [4] A. Adare *et al.*, *Phys. Rev. C* **77**, 024912 (2008).
 - [5] L. Adamczyk *et al.*, *Phys. Lett. B* **722**, 55 (2013).
 - [6] B. Abelev *et al.*, *Phys. Rev. Lett.* **109**, 072301 (2012).
 - [7] M. B. Johnson *et al.*, *Phys. Rev. Lett.* **86**, 4483 (2001).
 - [8] V. Guzey, M. Strikman, and W. Vogelsang, *Phys. Lett. B* **603**, 173 (2004).
 - [9] R. Baier, D. Schiff, and B. G. Zakharov, *Annu. Rev. Nucl. Part. Sci.* **50**, 37 (2000).
 - [10] S. Gavin and R. Vogt, *Nucl. Phys.* **A610**, 442 (1996).
 - [11] R. L. Thews, *Eur. Phys. J. C* **43**, 97 (2005).
 - [12] R. L. Thews and M. L. Mangano, *Phys. Rev. C* **73**, 014904 (2006).
 - [13] A. Andronic, P. Braun-Munzinger, K. Redlich, and J. Stachel, *Nucl. Phys.* **A789**, 334 (2007).
 - [14] A. Capella, L. Bravina, E. G. Ferreira, A. B. Kaidalov, K. Tywoniuk, and E. Zabrodin, *Eur. Phys. J. C* **58**, 437 (2008).
 - [15] P. F. Kolb and U. W. Heinz, in *Quark Gluon Plasma*, edited by R. C. Hwa and X. N. Wang (World Scientific, Singapore, 2003), pp. 634–714.
 - [16] P. Huovinen and P. V. Ruuskanen, *Annu. Rev. Nucl. Part. Sci.* **56**, 163 (2006).
 - [17] S. S. Adler *et al.*, *Phys. Rev. C* **72**, 024901 (2005).
 - [18] H. Hahn *et al.*, *Nucl. Instrum. Methods Phys. Res., Sect. A* **499**, 245 (2003).
 - [19] K. H. Ackermann *et al.*, *Nucl. Instrum. Methods Phys. Res., Sect. A* **499**, 624 (2003).
 - [20] B. Bonner, H. Chen, G. Eppley, F. Geurts, J. Lamas-Valverde, Ch. Li, W. J. Llope, T. Nussbaum, E. Platner, and J. Roberts, *Nucl. Instrum. Methods Phys. Res., Sect. A* **508**, 181 (2003).
 - [21] W. J. Llope *et al.*, *Nucl. Instrum. Methods Phys. Res., Sect. A* **522**, 252 (2004).
 - [22] M. Beddo *et al.*, *Nucl. Instrum. Methods Phys. Res., Sect. A* **499**, 725 (2003).

- [23] M. Anderson *et al.*, *Nucl. Instrum. Methods Phys. Res., Sect. A* **499**, 659 (2003).
- [24] A. M. Poskanzer and S. A. Voloshin, *Phys. Rev. C* **58**, 1671 (1998).
- [25] H. Masui and A. Schmah, [arXiv:1212.3650](https://arxiv.org/abs/1212.3650).
- [26] J. Gaiser, Ph.D. thesis, Stanford University, appendix F [Report No. SLAC-R-255, 1982 (unpublished)].
- [27] N. Borghini and J. Y. Ollitrault, *Phys. Rev. C* **70**, 064905 (2004).
- [28] J. Adams *et al.*, *Phys. Rev. Lett.* **93**, 252301 (2004).
- [29] J. Adams *et al.*, *Phys. Rev. Lett.* **92**, 062301 (2004).
- [30] B. I. Abelev *et al.*, *Phys. Rev. Lett.* **99**, 112301 (2007).
- [31] L. Yan, P. Zhuang, and N. Xu, *Phys. Rev. Lett.* **97**, 232301 (2006).
- [32] V. Greco, C. M. Ko, and R. Rapp, *Phys. Lett. B* **595**, 202 (2004).
- [33] X. Zhao and R. Rapp, [arXiv:0806.1239](https://arxiv.org/abs/0806.1239).
- [34] Y. Liu, N. Xu, and P. Zhuang, *Nucl. Phys.* **A834**, 317c (2010).
- [35] U. W. Heinz and C. Shen, (private communication).
- [36] L. Ravagli and R. Rapp, *Phys. Lett. B* **655**, 126 (2007).